Gain Enhancement of a Pyramidal Horn Using E- and H-Plane Metal Baffles

Matthew A. Koerner, *Member, IEEE,* and Robert L. Rogers, *Senior Member, IEEE*

***Abstract*—A technique for enhancing the gain of a wide-flare angle pyramidal horn is described. The gain of the antenna is increased by placing simple metal strips or baffles inside the horn near its throat. Two baffles, an E- and an H-plane baffle, are described and analyzed. The baffles are first analyzed through two-dimensional (2-D) numerical calculations and then through measurements in an experimental X-band horn. Each baffle enhances the antenna's gain in the respective plane. When the baffles are implemented together the gain enhancement is additive in decibels. The numerical calculations and measurements show that baffles can be used to significantly reduce the size of pyramidal horn antennas.**

***Index Terms*—Antenna gain, horn antennas.**

I. Introduction

With the dramatic increase in low-cost portable microwave and millimeter wave communications and sensing systems, there is a growing need for inexpensive, simple, compact, directional antennas. Large phased arrays, parabolic reflectors, and lensed horns are often used in systems needing high-gain antennas; but size, cost, and simplicity may be more important than antenna gain in many cases. In such cases, a simple antenna such as a pyramidal horn may be adequate. Unfortunately, even medium-gain pyramidal horns may be too long to be practical; thus, horn lenses are often used.

This paper presents a new technique for improving the performance of a wide-flare pyramidal horn antenna without the added cost and complexities associated with conventional horn lenses. When metallic baffles are placed inside the horn near its throat the antenna's performance is improved significantly. The metal baffles are simple planar structures that reduce phase curvature at the aperture like a lens. They were developed through calculations with two-dimensional (2-D) models of the horn's E- and H-planes. This loading technique is economical and very easy to implement.

In earlier work presented in Silver [1], the insertion of a thin metallic strip into a horn is briefly discussed. The metallic strip is reported to improve the E-plane directivity of a horn, but it is suggested that mismatch problems make the technique impractical. The idea in Silver is similar to our work with baffles, but the strip in Silver is oriented differently and it is unclear where the strip is placed in the horn and what its dimensions are. Numerical techniques such as those used in the development and analysis of our antennas were not readily available. The absence of these tools may have hindered further investigation at that time.

We will focus on one particular set of baffles that greatly enhance the performance of a wide-flare X-band pyramidal horn. Our previous work [2]–[4] and new results are combined into a comprehensive summary through the analysis of these baffles. The set contains two baffles that were designed independently through 2-D numerical modeling. One baffle was designed to enhance E-plane characteristics of the antenna and the other was designed to enhance H-plane characteristics. The 2-D numerical results approximate the true measured behavior of the antenna in the corresponding planes. When the two baffles are used together as a combination baffle their performance becomes additive. Clenet and Shafai [5] have also extended these ideas to conical horns based on our work.

In Section II, the pyramidal horn is reviewed to identify its critical parameters and their effects on the antenna's performance. The review describes the horn's radiating characteristics and why phase correcting devices must be used with short, wide-flare horns. The wide-flare X-band horn is described in Section III along with the 2-D models used to analyze the horn and simple horn loads. In Section IV, the 2-D numerical results for the baffle loaded X-band antenna are presented and discussed. In this section, a metal baffle for the E- and H-planes are described and performances of the antenna with and without the baffles are compared. In Section V, measured performances of the antenna fitted with physical interpretations of the metal baffles are presented and analyzed. These measurements include the antenna loaded with the E- and H-plane baffles independently and together as a combination baffle.

II. Pyramidal Horn

The pyramidal horn is a directional antenna that is widely used in microwave and millimeter wave systems. It is most commonly used as a calibration standard due to its robustness and predictability. Its simplicity makes it easy to construct, easy to use, and less expensive than most microwave antennas. The pyramidal horn's intrinsic utility has also been complemented by extensive research [6]. These qualities comprise the reasons our research focused on the pyramidal horn.

A. Pyramidal Horn Configuration

The pyramidal horn is a rectangular aperture antenna which has the geometry shown in Fig. 1. The conventions in Fig. 1 are commonly used and are very similar to those used in [7]. The antenna is simply an extension of the feeding waveguide. It transitions the waveguide aperture to a suitable size for directional

Manuscript received August 27, 1998; revised November 12, 1999.

The authors are with the Applied Research Laboratories, The University of Texas at Austin, Austin, TX 78713-8029 USA.

Publisher Item Identifier S 0018-926X(00)03270-1.

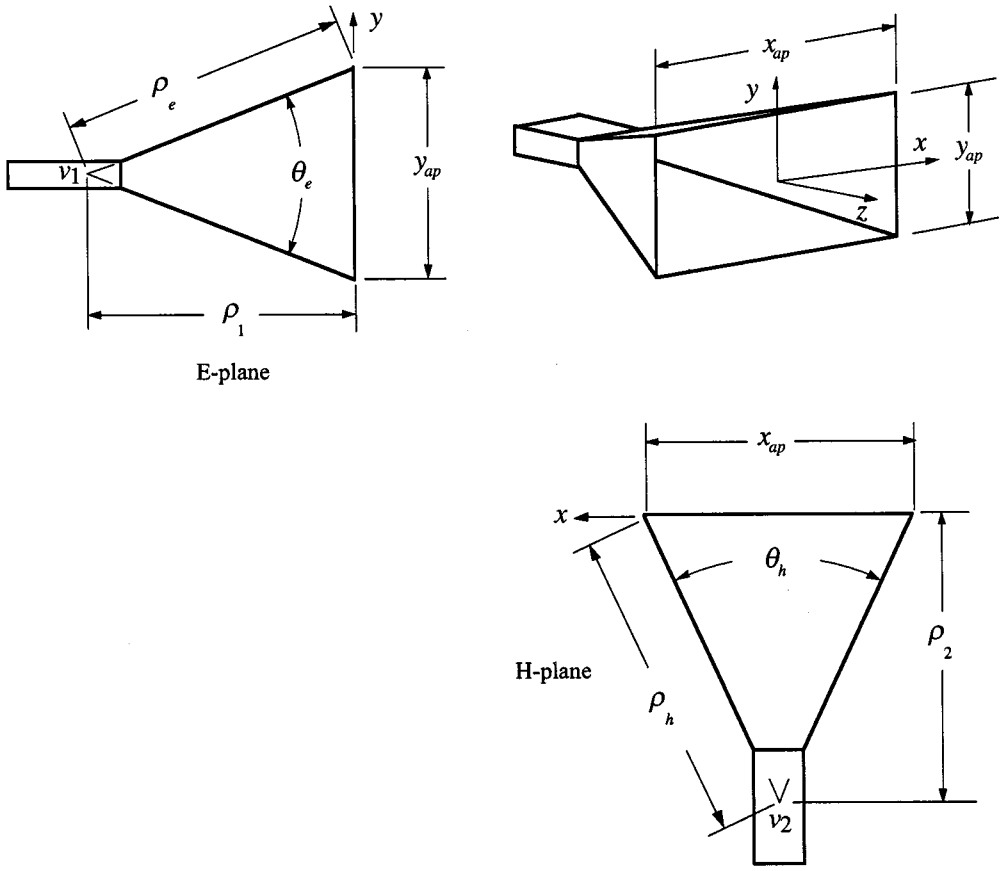

Fig. 1. Pyramidal horn.

transmission or reception of electromagnetic energy. The horn flares with flare angles θ_e in the E-plane and θ_h in the H-plane. Directivity is provided in the E- and the H-planes by the rectangular planar aperture. The aperture's dimensions are x_{ap} in the x-direction and y_{ap} in the y-direction. The slant heights ρ_e and ρ_h describe the length of the horn's sides from imaginary vertices at ν_1 and ν_2, respectively, to the aperture.

B. Aperture Field Effects

For lossless rectangular apertures the aperture efficiency equals 100% when the aperture electric fields are vertically polarized with a uniform amplitude distribution and a flat phase distribution [8]. The aperture fields for pyramidal horns have a TE_{10} amplitude distribution [7]. This mode effectively applies a tapered shading function to the aperture that reduces the sidelobes and broadens the main beam in the H-plane. With a flat phase distribution and a TE_{10} amplitude distribution, the aperture efficiency of a rectangular aperture is reduced to 81% [8].

The horn's flare angles cause the distance from the waveguide to different locations on the aperture to vary. Increasing the flare angles causes more variance between these paths. From Fig. 1 we see that the greatest path difference in the E-plane is $\rho_e - \rho_1$ and the greatest difference in the H-plane is $\rho_h - \rho_2$. These differences cause the wavefront at the aperture to be curved with a quadratic phase distribution. The fields across an aperture with a flat phase distribution add constructively in the direction of the main beam; a quadratic distribution weakens this constructive interference. Thus, increasing the flare angles increases phase curvature and lowers the aperture's directivity and aperture efficiency. The TE_{10} amplitude taper in the H-plane reduces the fields near the aperture edges where the phase deviates most from a flat distribution. Therefore, most of the benefit from reducing phase curvature in pyramidal horn antennas is realized in the E-plane.

The flare angles of a pyramidal horn can be chosen to optimize directivity for a given set of slant heights. A horn with optimized flare angles is termed an optimum-gain horn. An optimum gain horn is the most size efficient, unaided pyramidal horn antenna. However, optimum-gain horns can be too large for small systems needing a high-gain antenna. To increase the gain of a pyramidal horn, the slant heights must be extended to increase the aperture area and the flare angles must be reduced to offset the added phase curvature. Adding 3 dB to the gain of an optimum gain horn requires increasing the aperture area and slant heights of the horn by a factor of two [9].

Since the directivity of an aperture antenna is proportional to its aperture area, a short, compact, high-gain pyramidal horn would have to employ wide-flare angles. However, the flare angles of a pyramidal horn can not be larger than the angles describing an optimum-gain horn or the antenna directivity will be adversely affected. Therefore, some type of phase correcting device must be used with wide-flare pyramidal horns to improve their performance.

TABLE I
DIMENSIONS OF WIDE-FLARE X-BAND PYRAMIDAL HORN

E-plane Dimensions	H-plane Dimensions
$y_{ap} = 14.0\ cm$	$x_{ap} = 16.7\ cm$
$\rho_e = 18.5\ cm$	$\rho_h = 20.2\ cm$
$\rho_1 = 17.1\ cm$	$\rho_2 = 18.4\ cm$
$\theta_e = 45^\circ$	$\theta_h = 49^\circ$

III. EXPERIMENTAL HORN AND NUMERICAL MODELS

A. Construction

A wide-flare horn was constructed using an M/A-Com, MA-86 551 X-band antenna as a base antenna. The MA-86 551 is a simple, inexpensive ($20), metal-coated plastic antenna with a nominal gain over the X-band of 17 dB. The walls of the antenna were extended with single clad printed circuit board to enlarge the aperture area. The extensions were secured to each other and to the base antenna with copper foil tape. The dimensions of the antenna are shown in Table I. Constructing an experimental horn in this fashion is quick, simple, and inexpensive. The flare angles of the experimental antenna are greater than optimum so the antenna performance is limited by phase curvature. The performance of this antenna is analyzed in Sections IV and V through numerical and measured data.

B. Two-Dimensional Numerical Models

The E-plane and H-plane 2-D models of the pyramidal horn are based on a moment method solution to the magnetic field integral equation (MFIE) and the electric field integral equation (EFIE), respectively, [2], [10], [11]. Both models allow simple metal objects to be placed inside the antenna. A three-dimensional (3-D) model is necessary to correctly analyze the pyramidal horn; however, the rigorous analysis of a 3-D pyramidal horn is much more complex than the 2-D analysis especially when scattering structures are loaded into the antenna. Although the pyramidal horn is not separable into E-plane and H-plane solutions, the 2-D models are useful for approximating the directive characteristics of the antenna in the respective planes.

Fig. 2 pictures the E- and H-plane 2-D models. The horn and metal baffles in both models are described as perfect electric conductor (PEC) structures that have infinite length in the z-direction. The infinite direction is chosen as z to follow radial waveguide conventions. An MFIE in the E-plane model is formed from the boundary conditions along the PEC surfaces in Fig. 2(a) [11],

$$J_c(\rho,\varphi)|_{\mathrm{PEC}} + \frac{jk_o}{4}\int_C J_c(\rho',\varphi')\cos(\psi') \cdot H_1^{(2)}(k_oR)\,dc'\Big|_{\mathrm{PEC}} = -H_z^i|_{\mathrm{PEC}}. \quad (1)$$

Equation (1) relates the total magnetic field at a point $P(\rho, \phi)$ on a PEC surface [C in Fig. 2(a)] to equivalent electric current densities J_c along the PEC surfaces. In (1), H_z^i is the incident field produced by the source $\overline{J}^{Src}$, the primed coordinates indicate the source location and $H_1^{(2)}$ is the first-order Hankle function of the second kind [12]. The equivalent currents are all polarized in the c-direction defined by the unit vector $\hat{c} = -\hat{n} \times \hat{z}$ where $\hat{n}$ is the outward pointing normal to C. Similarly, an EFIE in the H-plane model is formed that relates the electric field to

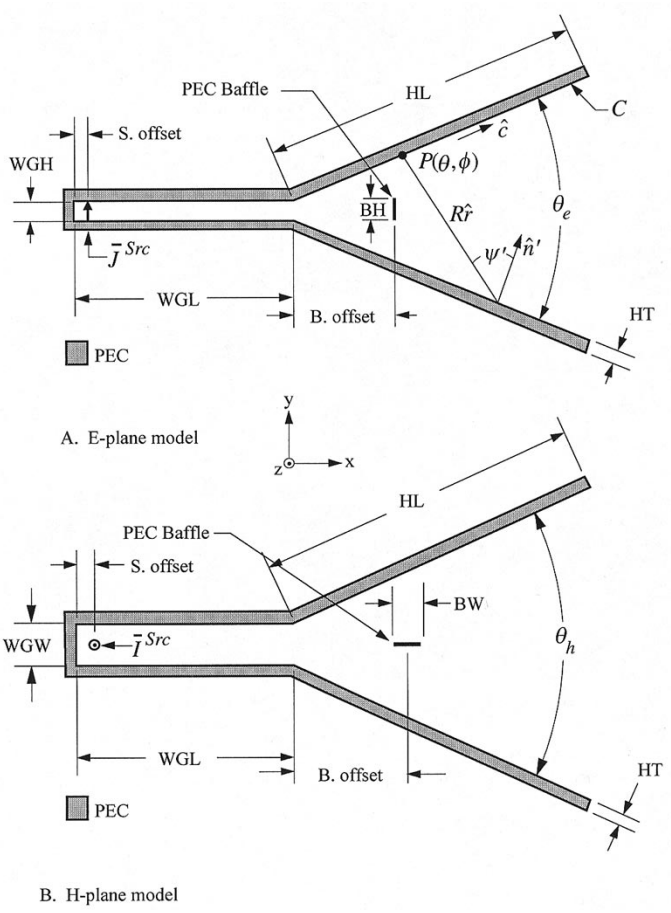

Fig. 2. 2-D models. (a) E-plane model. (b) H-plane model.

TABLE II
DIMENSIONS USED IN TWO-DIMENSIONAL MODELS

E-plane model dimensions	H-plane model dimensions
WGH = 0.35λ (10.3 GHz)	WGW = 0.8λ
WGL = 4.0λ	WGL = 4.0λ
S. offset = 0.25λ	S. offset = 0.25λ
HL = 5.9λ	HL = 6.0λ
HT = 0.2λ	HT = 0.2λ
BH = 0.5λ	BW = 0.5λ
B. offset = 2.1λ	B. offset = 2.0λ
$\theta_e = 45^\circ$	$\theta_h = 49^\circ$

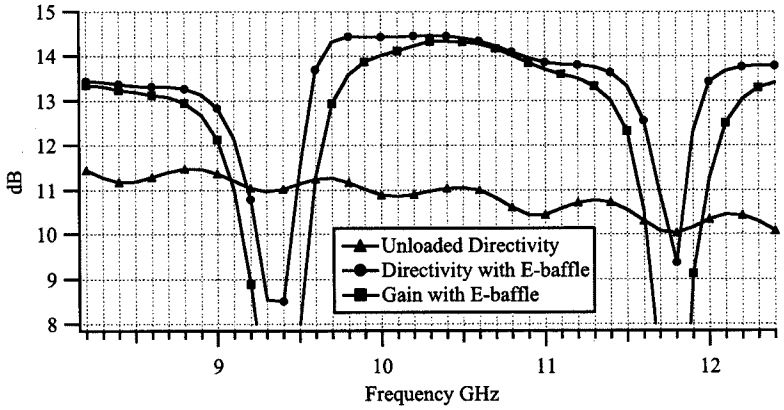

Fig. 3. E-plane calculated on-axis directivity and gain.

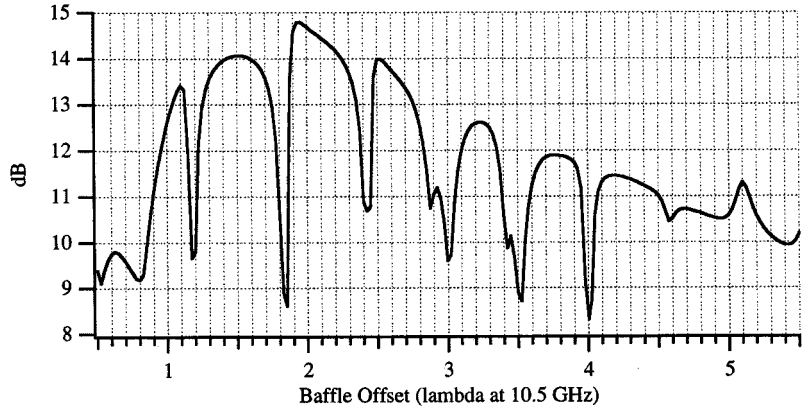

Fig. 4. E-plane calculated directivity versus baffle offset at 10.5 GHz.

equivalent surface currents along the PEC surfaces in Fig. 2(b) [11]

$$\frac{\omega\mu_o}{4}\int_C J_z(\rho',\phi')H_0^{(2)}(k_oR)\,dc'\bigg|_{\rm PEC} = E_z^i(\rho,\phi)|_{\rm PEC}. \tag{2}$$

In (2), the equivalent currents are all polarized in the z-direction, E_z^i is the electric field produced by the source $\overline{I}^{Src}$, and $H_0^{(2)}$ is the zero-order Hankle function of the second kind [12].

The equivalent currents are then calculated by solving (1) and (2) using the moment method [10], [11]. We chose a pulse-expansion and point-matching moment method solution in which the currents are expanded into rectangular basis functions and the boundary conditions are matched at the center of each basis. The integral over each basis was calculated using a rectangular approximation except for the self terms where limiting approximations were necessary [2].

Field values, directivity, gain, reflection efficiency, and beam patterns in both models are calculated from the equivalent currents [2]. The far fields are calculated directly from the equivalent currents and source using far-field approximations and the beam patterns and directivity are calculated from the far fields. The gain is related to the directivity by $G = \varepsilon_t D_o$ where ε_t is the total antenna efficiency [13]. In the following numerical results, only reflection-losses are considered and ε_t is equal to the reflection efficiency $(1 - |\Gamma^2|)$ where the current reflection coefficient Γ is calculated from the current standing wave pattern in the waveguide.

In order to calculate results over the entire X-band in the E-plane model, the dimensions, and locations of the E-plane horn [shown in Fig. 2(a)] were entered in units of wavelength at 10.3 GHz and scaled appropriately for calculations at other frequencies. The basis functions along the horn were chosen to be 0.1 λ (10.3 GHz) long everywhere except on the waveguide end. The bases on the waveguide end are 0.025 λ long to resolve the waveguide height. The E-plane baffle is a thin vertically oriented PEC strip placed near the horn's throat. The length of the bases forming the baffle are 0.05 λ long in order to resolve the small structure. The baffle is only one basis function thick representing a thin object. Dimensions of the horn and baffle used for numerical results are shown in Table II.

The H-plane baffle, shown in Fig. 2(b), is a thin PEC object centered horizontally in the narrow end of the horn. The size of the horn basis functions in this model are all 0.1 λ (10.3 GHz) long and the baffle basis functions are 0.05 λ. Table II lists the H-plane horn and baffle's dimensions.

IV. Numerical Results

A. E-Plane Numerical Results

The E-plane directivity and gain of the X-band horn were calculated at 100 MHz intervals from 8.2–12.4 GHz using the

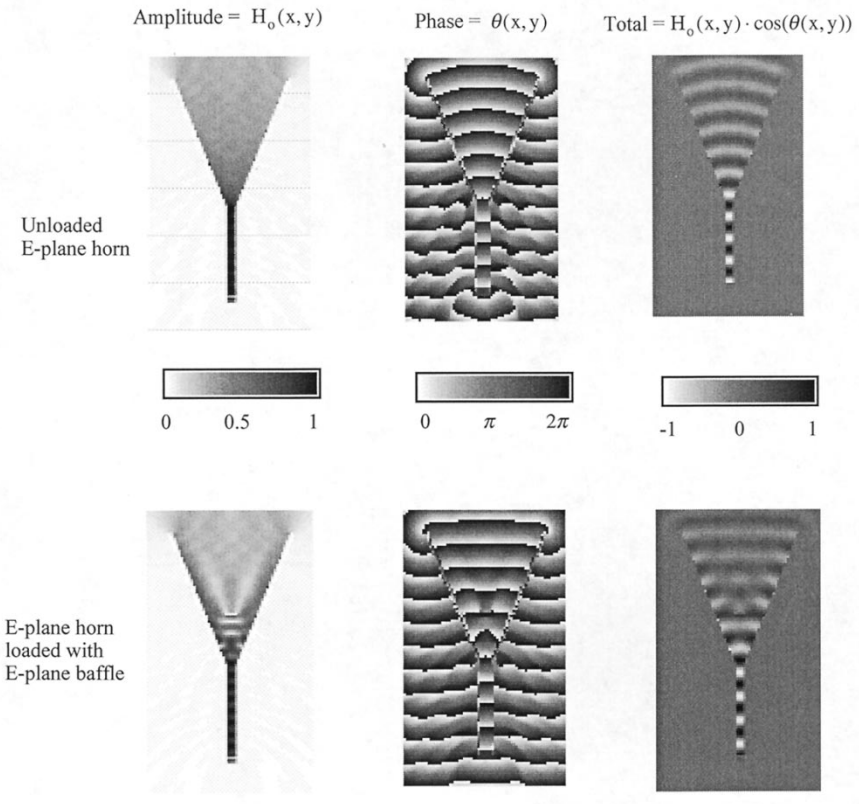

Fig. 5. Calculated E-plane interior magnetic fields at 10.5 GHz.

2-D E-plane model. The results are plotted in Fig. 3. The figure displays results for the unloaded antenna and the antenna loaded with the E-plane baffle. The calculations show that the baffle increases the antenna gain by 3 dB over the frequency range from 10.0–11.1 GHz. This enhancement band corresponds to a bandwidth of 10.4%. The directivity is increased by 3 dB from 9.7 to 11.2 GHz.

The antenna's performance is dependent upon the baffle's electrical distance from the horn's throat along the antenna's axis—the baffle offset [*b. offset* in Fig. 2(a)]. Fig. 3 shows that the reflection efficiency and the directivity begin to decrease near 8.8 GHz, reach a null at 9.4 GHz and recover by 10.0 GHz. The baffle offset equals 1.8 λ at 8.8 GHz and 2.0 λ at 10.0 GHz. The offset ranges from 2.0–2.26 λ over the enhancement band (10.0 to 11.1 GHz) and ranges from 2.2–2.5 λ over the second null band (11.1–12.4 GHz). These electrical distances show that the length of the enhancement and null bands correspond to baffle offsets ranging over approximately one quarter of a wavelength. The center frequency of the enhancement band corresponds to an offset of approximately 2.15 λ so the center frequency can be adjusted by adjusting the baffle offset.

Fig. 4 shows directivity calculations versus baffle offset at 10.5 GHz in the E-plane model. The baffle was moved along the antenna's axis starting at an offset of 0.5 λ in 0.025 λ increments to 5.0 λ. The nulls in the directivity occur at baffle offsets of 1.2, 1.7, 2.4, 3.0, 3.5, and 4.0 λ. The distance between each null is approximately 0.5 λ.

The enhancement band is centered at 10.5 GHz. At this frequency the loaded horn matches well with the waveguide and the baffle adds 3.2 dB to the antenna gain. (A small reflection loss and a consequently small difference between directivity and gain indicate a good impedance match.) The interior magnetic fields are plotted in Fig. 5 for the loaded and unloaded antennas at this frequency. The fields are sampled at 0.1 λ intervals in the x- and y-directions. The gray scale used in the amplitude plots is a relative scale where black signifies 1 A/m and white signifies 0 A/m. In the phase plot, white to black bands correspond to 360° of phase shift. The third field plot pictures the total field at

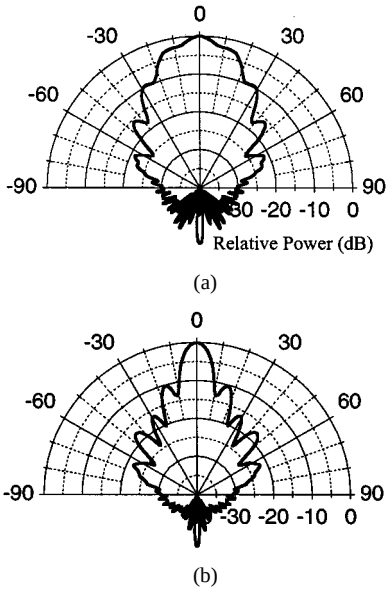

Fig. 6. Calculated E-plane beam patterns at 10.5 GHz. (a) Unloaded E-plane. (b) Loaded E-plane.

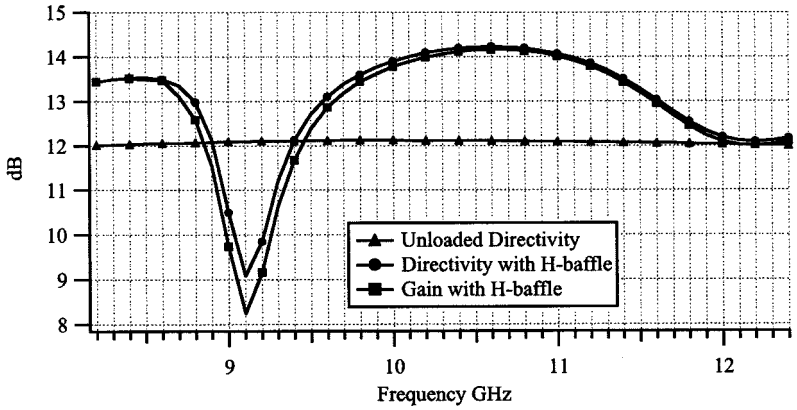

Fig. 7. H-plane calculated on-axis directivity and gain.

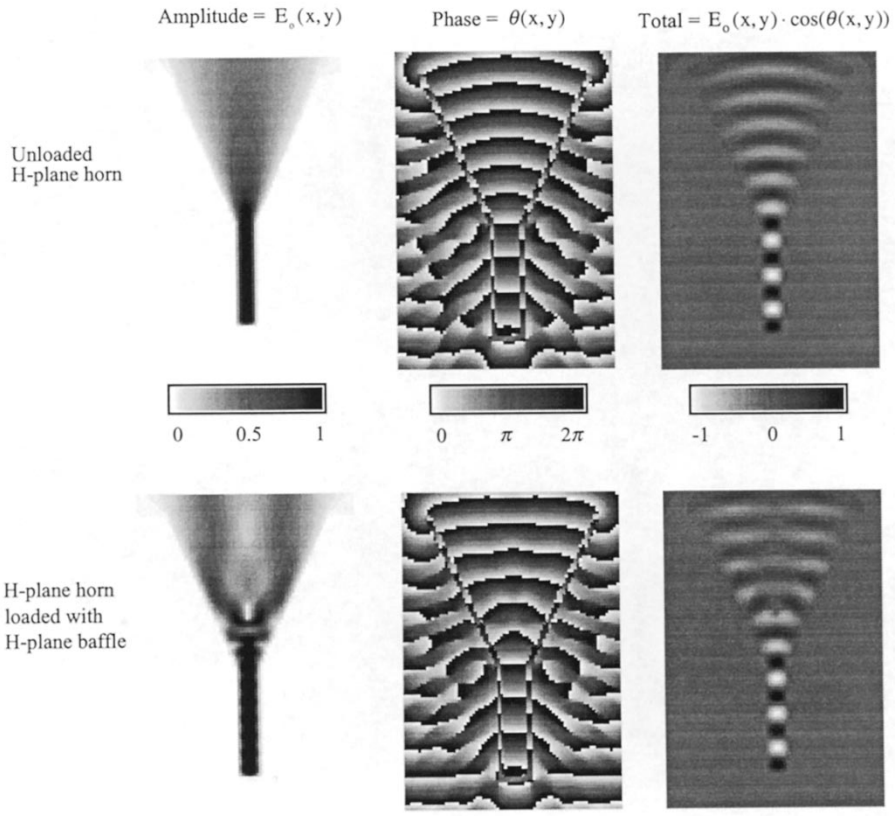

Fig. 8. Calculated H-plane interior electric fields at 10.5 GHz.

time zero or $\mathrm{Re}\{H_z(x, y)e^{j\omega t}|_{t=0}\} = H_o(x, y)\cos(\theta(x, y))$ where $H_o(x, y)$ is the amplitude and $\theta(x, y)$ is the phase of the magnetic field at the location x, y.

The aperture amplitude distribution of the unloaded horn is fairly uniform, but a quadratic phase distribution is revealed in the phase plot. The phase at the edge of the aperture differs from the phase at the center by approximately 180°. The loaded field plots show that the baffle corrects the phase curvature and has little effect on the amplitude distribution. Fields emitted from the waveguide are forced to travel around either side of the baffle forming two radiating slots the feed the remainder of the horn. The two slots feed the remainder of the antenna. The fields from the two slots interfere to produce a relatively flat phase distribution and uniform amplitude distribution at the aperture. We can also look at this phenomenon a little differently [2]. It appears that the baffle delays the fields in the central region of the horn. The delay adds length to the central path so that this path is equivalent to the paths near the edges of the horn. As the fields spread past the baffle the central and edge fields reach the aperture in phase.

In the frequency bands where nulls appear in the directivity in Fig. 3, standing wave patterns form nulls in the slots on either side of the baffle and a maximum in front of the baffle. Most of the energy appears to radiate from the maximum in front of the baffle in the null bands resulting in poor antenna performance.

The E-plane beam patterns of the loaded and unloaded antennas at 10.5 GHz are shown in Fig. 6. The effects of phase curvature are apparent in the unloaded beam pattern. The main

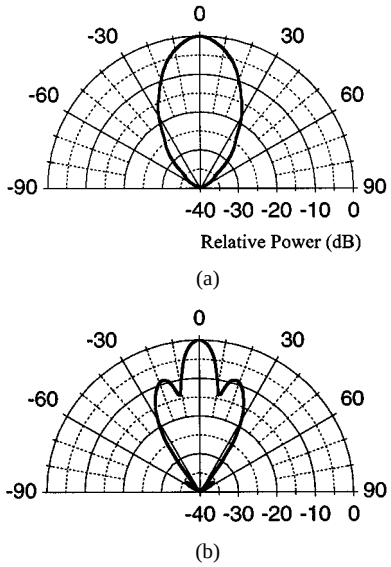

Fig. 9. Calculated H-plane beam patterns at 10.5 GHz. (a) Unloaded H-plane. (b) Loaded H-plane.

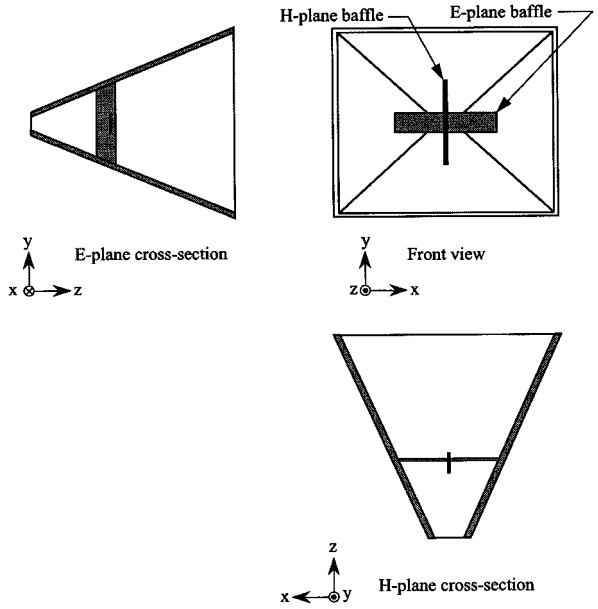

Fig. 10. Working drawing of pyramidal horn loaded with combination baffle.

beam is very broad and the sidelobes are not distinct. Loading the antenna with the E-plane baffle decreases the aperture phase curvature resulting in more on-axis constructive interference. The main lobe is narrowed and the nulls between sidelobes become deeper. The 3-dB beamwidth of the loaded horn is 10 degrees and the unloaded horn's beamwidth is 28°. Additionally, the first sidelobes of the loaded horn are 10 dB down from the main beam and the remaining sidelobes are all 15 dB below the main beam.

B. H-Plane Numerical Results

Fig. 7 shows that the H-plane baffle increases the antenna gain and directivity 1.9 dB over an 700 MHz band centered around 10.6 GHz. The gain and directivity are very similar implying that the loaded horn's input impedance is well matched to the waveguide over the entire X-band. The H-plane baffle does not provide as much performance enhancement as the E-plane baffle, but this baffle configuration can be combined with the E-plane baffle to improve the overall antenna performance. This will be shown through measured results in Section V. A baffle parallel to the aperture in the H-plane will produce results similar to those produced by the E-plane baffle. However, a baffle configuration was not found that enhances the antenna's performance with both baffles parallel to the aperture.

The null in directivity centered at 9.1 GHz corresponds to the center of the baffle being placed 1.75 λ in front of the horn's throat. At the frequencies near 9.1 GHz energy radiating through the antenna does not flow smoothly around the baffle. The fields around the baffle produce an aperture distribution with a phase reversal in its central region. The distribution resembles a TE_3 mode with an added quadratic phase term.

The antenna reaches its peak directivity near 10.5 GHz. The interior electric fields at this frequency are plotted in Fig. 8. The aperture amplitude distribution of the unloaded horn appears to be the half period of a sinusoid indicative of the TE_1 parallel-plate waveguide mode, and the phase distribution is quadratic due to spreading inside the horn. The TE_1 mode is analogous to the TE_{10} mode in a 3-D rectangular waveguide. A new mode is setup when the baffle is added which appears to be the combination of odd ordered modes. The new mode illuminates the aperture more evenly than the TE_1 mode. The baffle also flattens the phase by forcing the energy to diffract around the baffle similar to the effect produced by the E-plane baffle.

The calculated beam patterns at 10.5 GHz of the unloaded and loaded H-plane horns are shown in Fig. 9. Like the TE_{10} distribution in a 3-D horn, the unloaded horn's TE_1 amplitude distribution effectively reduces the size of the aperture and limits phase curvature effects. This distribution produces one broad beam with a 3-dB beamwidth of 20°. Since the H-plane baffle redistributes the amplitude and reduces the phase curvature, the beam pattern of the loaded horn has a narrow main lobe and distinctive sidelobes. The beamwidth of the main lobe is 10° and the sidelobes are 9 dB down from the main lobe.

V. Experimental Results

A. Setup

The baffles were fabricated from 0.7-mm copper sheet for measurement of the loaded horn's performance. The E-plane baffle was cut to extend completely across the horn in the direction (x in Fig. 1) corresponding to the infinite direction z in the E-plane model. Similarly, the H-plane baffle was cut to extend across the horn in the direction corresponding to z (y in Fig. 1) in the H-plane model. In order to make measurements with both baffles inside the horn, a slot was cut in the H-plane baffle so that the E-plane baffle could intersect it. This physical implementation of the combination E- and H-plane baffle is pictured in Fig. 10.

An M/A Com, MA-86 551 pyramidal horn was used as the transmitting antenna. Both the transmitting antenna and the test antenna (wide-flare X-band horn) were set 4.5 ft off the ground on plastic stands. The largest dimension of the test antenna's aperture is its diagonal D. The test antenna was placed 20 ft

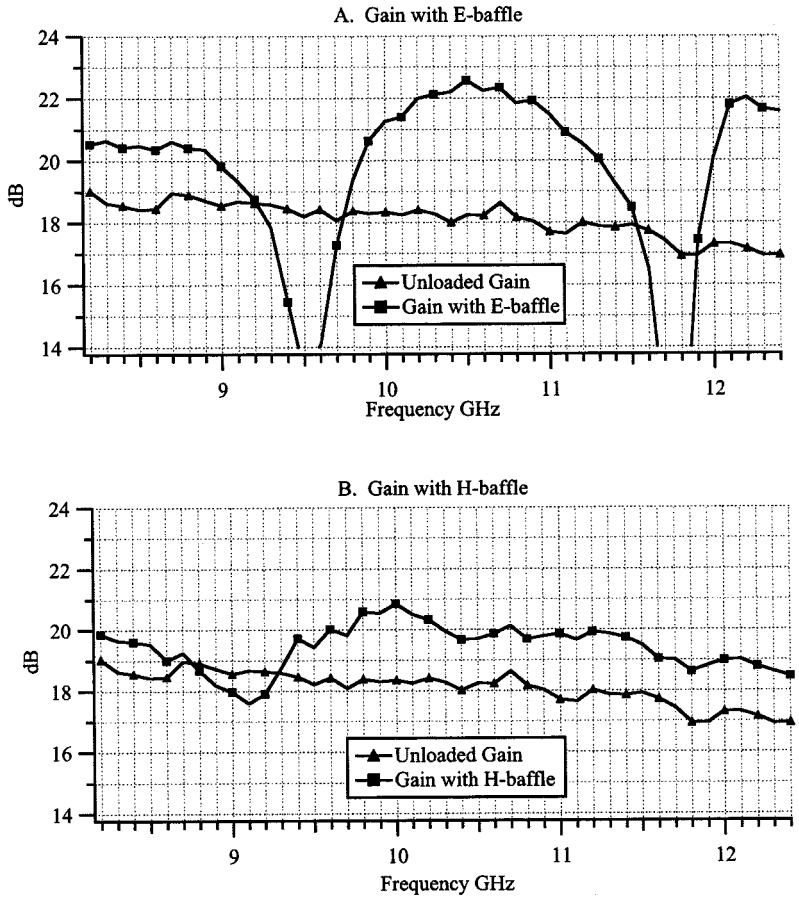

Fig. 11. Measured on-axis gain versus frequency for E-plane and H-plane baffle. (a) Gain with E-baffle. (b) Gain with H-baffle.

from the transmitter corresponding to a distance of $3.6\ D^2/\lambda$ at 10.5 GHz. The transmitting antenna was fed through an X-band coax-to-waveguide feed with a HP-8350B sweep oscillator. The test antenna's received power was measured through an X-band coax-to-waveguide feed using an Anritsu ML83A power meter and an Anritsu MA73A power sensor. For gain versus frequency measurements, the transmitting and test antennas were directed on axis and the received power was recorded at 100-MHz intervals from 8.2 to 12.4 GHz. Reflection coefficient measurements were made using the HP sweep oscillator, a direction coupler, and the Anritsu power meter.

Beam pattern measurements were measured at 10.5 GHz. The antenna stands rotated freely in the azimuthal direction only. Therefore, the antennas were oriented so their E- or H-planes were parallel to the ground when making the respective beam-pattern measurement. The test antenna was turned in 2.5° increments from −90 to 90°, and the received power was measured at each increment.

B. Measurements

The on-axis gain of the horn loaded with the E-plane baffle is shown in Fig. 11(a). The measurements agree with the 2-D calculated results shown in Fig. 3. The E-plane baffle enhances the gain by 3 dB over the unloaded horn in a 1 GHz band from 10.1 to 11.1 GHz. The bandwidth of this enhancement band is 9.4%. The peak gain in the enhancement band is 22.5 dB at 10.5 GHz and the average gain is 21.9 dB.

H-plane calculations shown in Fig. 7 also agree with the measured results shown in Fig. 11(b). The performance of this baffle is not as significant as the E-plane baffle, but the baffle increases the antenna gain by nearly 2 dB over the E-plane enhancement band.

In Fig. 12(a) the measured gain of the horn loaded with the combined baffles shows that the antenna gain is increased by 4.5 dB over a 900 MHz frequency band. This band ranges from 10.2–11.1 GHz and has a bandwidth of 8.5%. Over the 4.5 dB enhancement band, the gain peaks to 23.4 dB and the average gain is 23.1 dB. The baffles improve the antenna's gain by 5 dB over a 600 MHz band from 10.4 to 11.0 GHz. The gain never falls below 23 dB in this 5-dB enhancement band. The loaded horn's aperture efficiency, shown in Fig. 12(b), is greater than 50% from 10.1 to 11.0 GHz. The aperture efficiency stays above 55% from 10.2 to 10.9 GHz and peaks to 60.9% [aperture efficiency = $100 \times (\text{Gain}/4\pi(\text{Aperture Area})/\lambda^2)$].

The magnitude of the reflection coefficients, $|\Gamma|$, for the horn with and without the combination baffle are shown in Fig. 12(c). $|\Gamma|$ of the loaded antenna stays very close to −10 dB over most of the X-band. This result may be consistent with the mismatch problems mentioned in Silver [1], but Silver gives no quantitative data for matching. Matching in the 4.5-dB enhancement band would be acceptable for many applications. In the en-

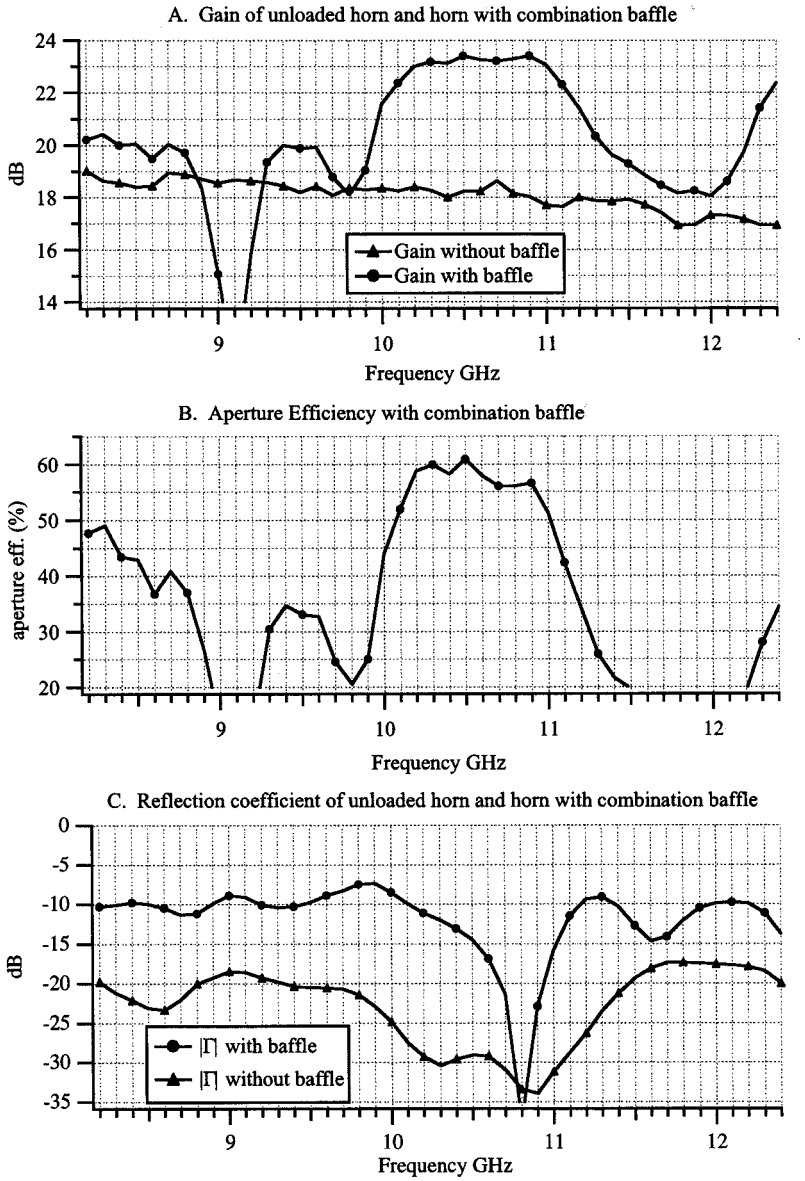

Fig. 12. Measured performance of horn with combination baffles. (a) Gain of unloaded horn and horn with combination baffle. (b) Aperture efficiency with combination baffle. (c) Reflection coefficient of unloaded horn and horn with combination baffle.

hancement band $|\Gamma|$ is less than -10 dB and the antenna has a resonance at 10.8 GHz.

The E- and H-plane beam patterns of the unloaded horn and the horn loaded with the combination baffle are shown in Fig. 13. The E- and H-plane beam patterns are very similar to those calculated and plotted in Figs. 6 and 9, respectively. The unloaded horn suffers from the effects of phase curvature and the TE_{10} waveguide mode. The half-power beamwidths of the unloaded horn are approximately 20° in both planes. The baffles produce a very symmetric main beam that has half-power beamwidths in the E- and H-planes equal to 10°.

C. Comparison to an Optimum-Gain Horn

Without the use of a horn load, the most compact horn design is an optimum-gain horn. Using the design equations in [9], the dimensions of an optimum-gain horn were calculated for an antenna gain of 23.1 dB. This gain value corresponds to the average gain of the wide-flare X-band horn with the combined baffles over the 4.5 dB enhancement band. The optimum-gain horn's dimensions are shown in Table III. The optimum-gain horn's calculated on-axis length (distance from the throat to the aperture) is 11.5 λ and its aperture area is 35.5 λ^2. Comparatively, at 10.5 GHz (the center of the 4.5 dB enhancement band) the wide-flare horn's length is 5.5 λ (see Table I) and its aperture area is 28.6 λ^2. These dimensions show that the wide-flare X-band horn is 52% shorter than the optimum gain horn and its aperture area is 19% smaller than the optimum gain horn's. The wide-flare horn is not only considerably smaller than the optimum-gain horn, its aperture efficiency is also greater; the wide-flare horn's aperture efficiency is over 55% and the optimum gain horn's aperture efficiency is 46%.

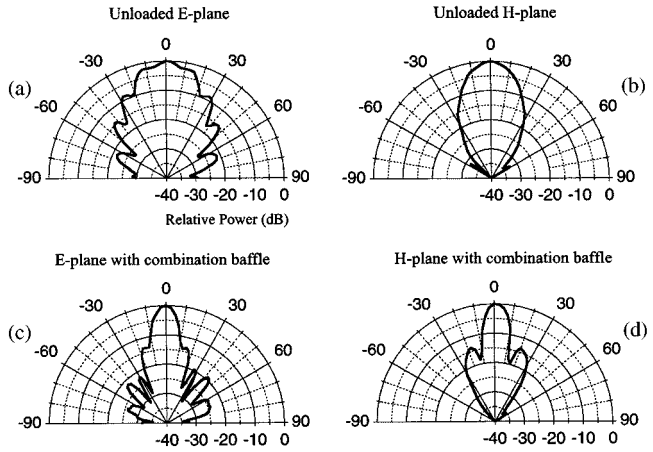

Fig. 13. Measured beam patterns at 10.5 GHz. (a) Unloaded E-plane. (b) Unloaded H-plane. (c) E-plane with combination baffle. (d) H-plane with combination baffle.

TABLE III
CALCULATED DIMENSIONS OF OPTIMUM GAIN HORN

$y_{ap} = 5.1\lambda$	$x_{ap} = 6.9\lambda$
$\rho_e = 12.6\lambda$	$\rho_h = 13.5\lambda$
$\theta_e = 23^o$	$\theta_h = 30^o$

VI. CONCLUSIONS

We developed an economical, compact, X-band, pyramidal horn antenna. The antenna utilizes metal baffles that enhance the antenna's performance by correcting phase curvature and modifying the aperture amplitude distribution. It was shown that metal baffles considerably enhance the antenna's performance over a frequency band of approximately 1 GHz. The baffles offer a simple means of shortening pyramidal horns without the use of lenses.

These results are preliminary and the topic has many avenues for further research. There are two characteristics of the antenna discussed in this paper that should be investigated further. First, the antenna's bandwidth and baffle relationship should be studied carefully. Improvements in the antenna's bandwidth would significantly improve its applicability. Second, the antenna is only a medium-gain antenna, and high-gain results may be possible with different baffle and horn configurations. The development of a 3-D model of the horn and baffles would allow us to study the antenna in more detail and produce better baffle configurations. The technique outlined here for using baffles has been applied successfully to conical horns [5] and could also prove to be effective in other configurations such as in millimeter-wave integrated-horn antennas [14], [15] where the flare angle is fixed.

REFERENCES

[1] S. Silver, *Microwave Antenna Theory and Design*, ser. MIT Radiation Lab. Ser.. New York: McGraw-Hill, 1949, vol. 12, p. 383.
[2] M. A. Koerner, "Gain enhancement of a wide-flare, X-band, pyramidal horn using metal baffles," Master's thesis, Univ. Texas, Austin, TX, Aug. 1996.
[3] M. A. Koerner and R. L. Rogers, "Gain enhancement of wide flare angle horn antennas using metallic baffles," in *URSI Nat. Radio Sci. Meet.*. Boulder, CO, Jan. 1996, oral presentation.
[4] M. A. Koerner and R. L. Rogers, "Enhancement of wide-flare pyramidal horn E- and H-plane performance using metal baffles," in *URSI North Amer. Radio Sci. Meet.*, Montreal, Canada, July 1997, oral presentation.
[5] M. Clenet and L. Shafai, "Gain enhancement of conical horn by introducing bodies of revolution inside the horn," in *IEEE AP-S Symp.*, Atlanta, GA, June 1998, pp. 1718–1721.
[6] A. W. Love, *Electromagnetic Horn Antennas*. New York: IEEE Press, 1976.
[7] C. A. Balanis, *Antenna Theory Analysis and Design*. New York: Wiley , 1982, ch. ch. 12.
[8] ——, *Antenna Theory Analysis and Design*. New York: Wiley, 1982, ch. 11.
[9] E. H. Braun, "Some data for the design of electromagnetic horns," *IEEE Trans. Antennas Propagat.*, vol. AP-4, pp. 29–31, Jan. 1956.
[10] R. F. Harrington, *Field Computation by Moment Methods*. New York: MacMillan, 1968, ch. 3.
[11] C. A. Balanis, *Advanced Engineering Electromagnetics*. New York: Wiley, 1982, ch. 12.
[12] R. F. Harrington, *Time-Harmonic Electromagnetic Fields*. New York: McGraw-Hill, 1961.
[13] C. A. Balanis, *Antenna Theory Analysis and Design*. New York: Wiley, 1982, ch. 2.
[14] G. V. Eleftheriades, W. Y. Ali-Ahmad, L. P. B. Katehi, and G. M. Rebeiz, "Millimeter-wave integrated-horn antennas—Part I: Theory," *IEEE Trans. Antennas Propagat.*, vol. 39, pp. 1575–1581, Nov. 1991.
[15] W. Y. Ali-Ahmad, G. V. Eleftheriades, L. P. B. Katehi, and G. M. Rebeiz, "Millimeter-wave integrated-horn antennas—Part II: Experiment," *IEEE Trans. Antennas Propagat.*, vol. 39, pp. 1582–1586, Nov. 1991.

Matthew A. Koerner (S'88–M'97) was born in Dayton, OH, in 1969. He received the B.S. degree from the University of Cincinnati, OH, in 1992, and the M.S. degree from the University of Texas at Austin, in 1996, both in electrical engineering.

He was with the Applied Research Laboratories, University of Texas at Austin, in 1992, where he is currently a Research Associate. His research there has involved microwave antenna design, millimeter-wave propagation studies, and microwave and millimeter-wave transceiver design. His current work and interests include antenna design, wireless communications, and wireless networking.

Robert L. Rogers (M'98–SM'99) was born in San Angelo, TX, in 1961. He received the B.S. degree in 1983, the M.S.E. degree in 1985, and the Ph.D. degree in 1989, all in electrical engineering from the University of Texas at Austin.

Upon graduation, he accepted a position at the Applied Research Laboratories, University of Texas at Austin, where he is currently a Principal Investigator. He has worked in the areas of microwave and millimeter-wave antennas, sensors and communications systems, as well as high-power pulsed energy systems. His research interests are in the areas of RF antennas, sensors, signal processing, wireless networking, and communications.